Bistability and transitions induced by topography in a laboratory model of a geostrophic jet

Joël Sommeria, Mani Mathur

LEGI

Grenoble

Atmospheric blocking

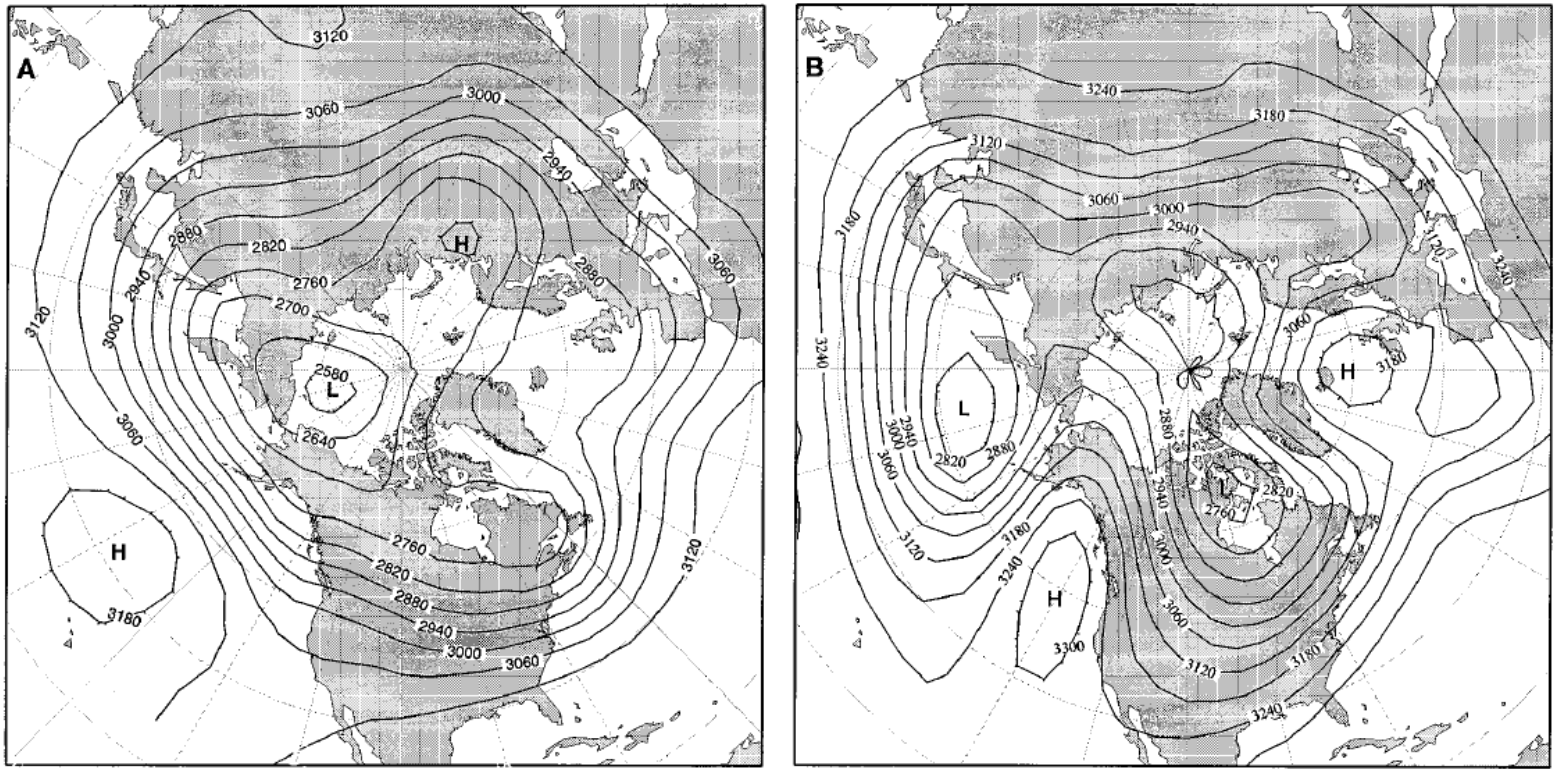

Fig. 1. Atmospheric pictures of (**A**) zonal and (**B**) blocked flow, showing contour plots of the height (m) of the 700-hPa (700 mbar) surface, with a contour interval of 60 m for both panels. The plots were obtained by averaging 10 days of twice-daily data for (A) 13 to 22 December 1978 and (B) 10 to 19 January 1963; the data are from the National Oceanic and Atmospheric Administration's Climate Analysis Center. The nearly zonal flow of (A) includes quasi-stationary, small-amplitude waves (*32*). Blocked flow advects cold Arctic air southward over eastern North America or Europe, while decreasing precipitation in the continent's western part (*26*).

Bistability of the Kuroshio current

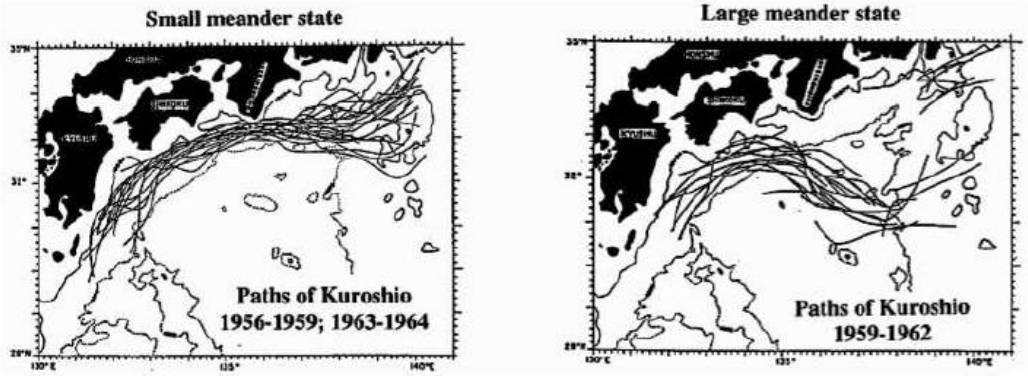

Figure 3: Bistability of the paths of the Kuroshio during the 1956-1962 period : paths of the Kuroshio in (left) its small meander state and (right) its large meander state. The 1000-m (solid) and 4000-m (dotted) contours are also shown. (figure from Schmeits and Dijkstraa [47], adapted from Taft 1972.)

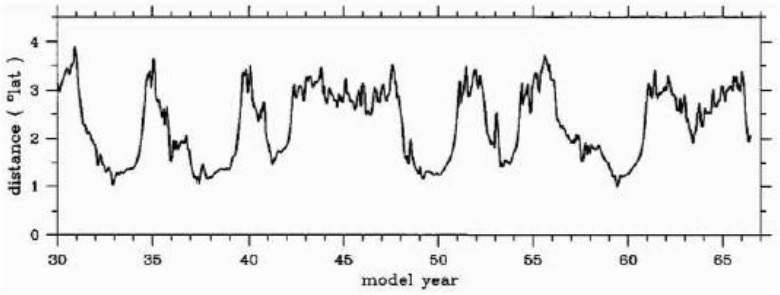

Figure 4: Bistability of the paths of the Kuroshio, from Qiu and Miao [41] : timeseries of the distance of the Kuroshio jet axes from the coast, averaged other the part of the coast between 132°-140°E, from a numerical simulation using a two layer primitive equation model.

Two theoretical approaches to bi-stability

- Low dimensional dynamical systems (few degrees of freedom), for instance:
  - Lorenz model.
  - Ice-atmosphere interaction seen as a ‘simple’ dynamical model (D. Paillard, 1998, *Nature)*

- Equilibrium statistical mechanics with phase transition (many degrees of freedom).
Self-organisation of 2D turbulence at large scale

‘condensation’ of the inverse energy cascade

J. Sommeria, J. Fluid Mech. 1986

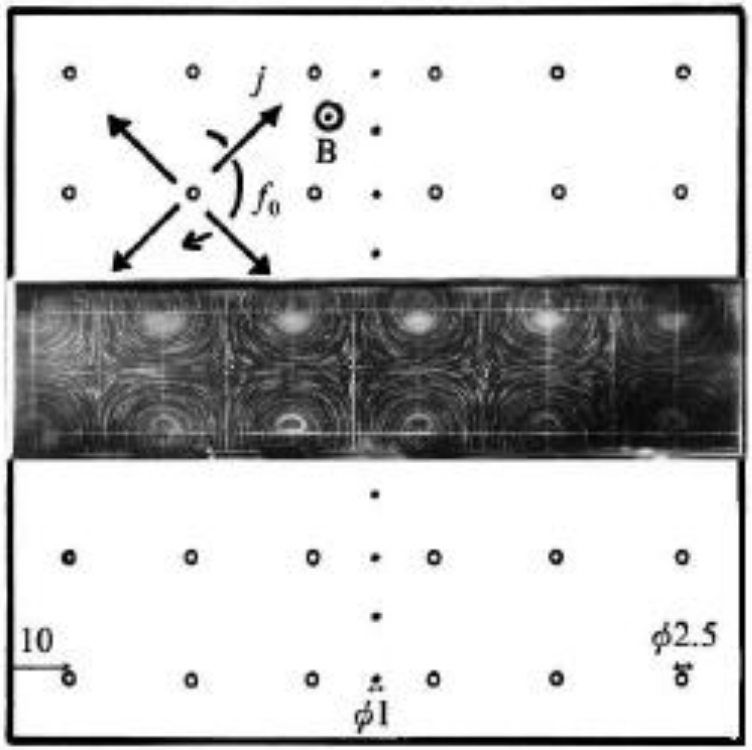

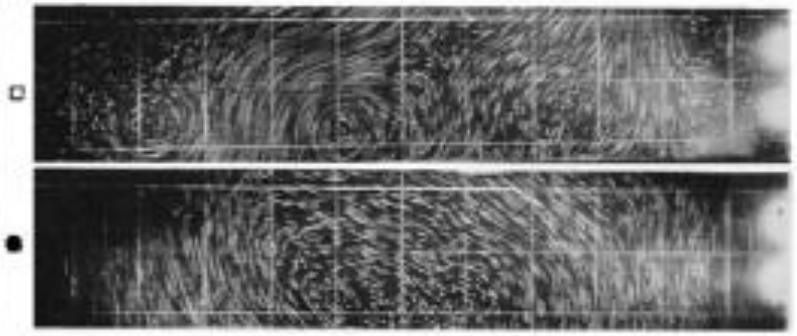

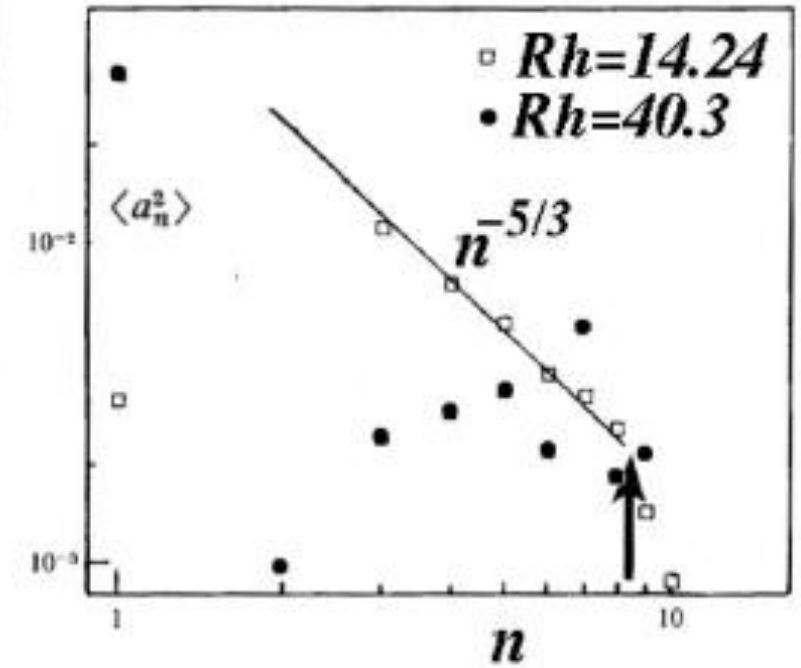

Bistability of the global circulation

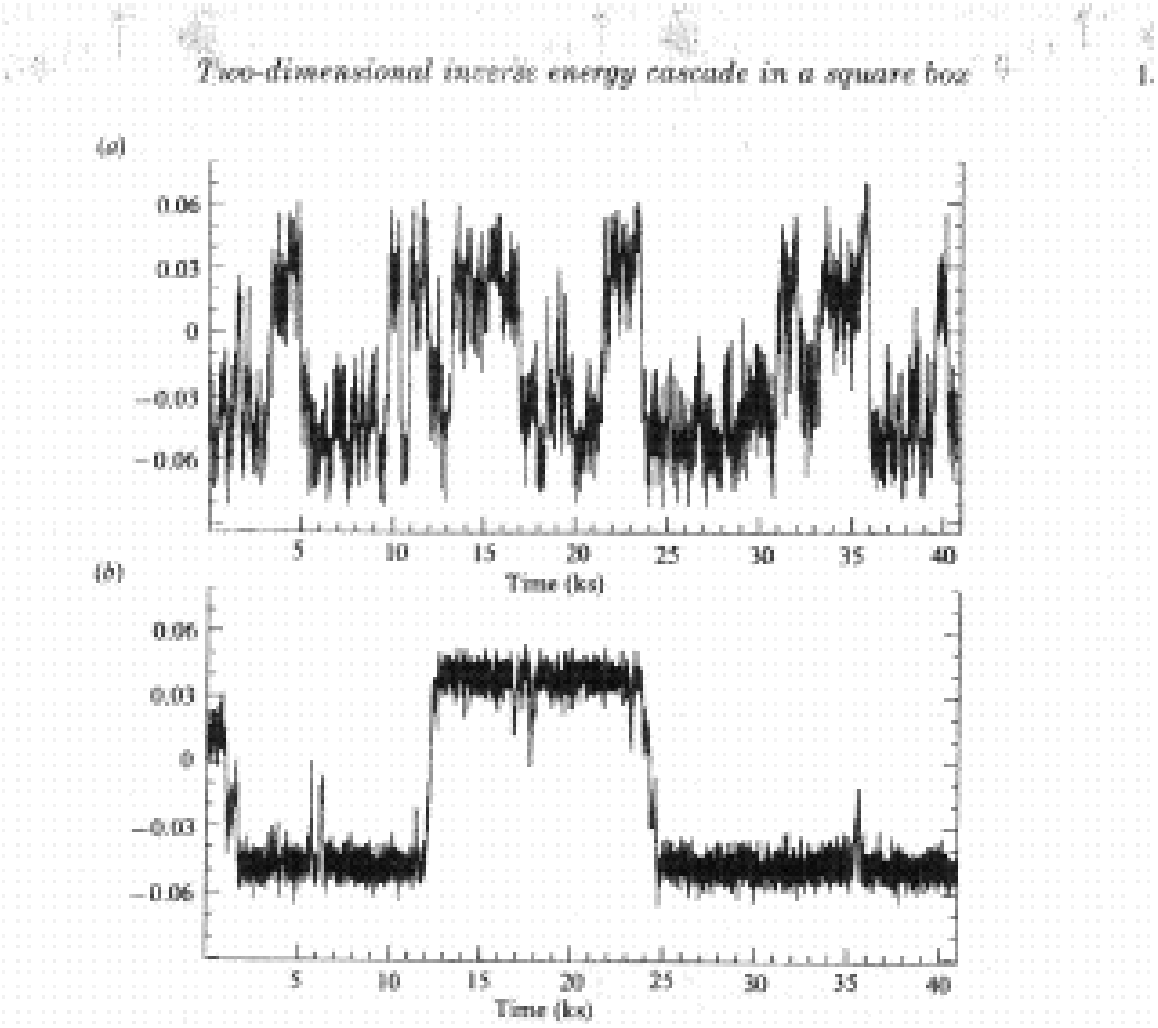

FIGURE 13. Typical time records of the non-dimensional central stream function (free surface $l = 16$ A). (a) $Rb = 36.8$; (b) $Rb = 39.5$. Notice the very long timescales.

Statistical mechanics of vorticity

Onsager (1949), Miller(1990), Robert (1990), Robert and Sommeria (1991)

2D Euler equations.

- Conservation of the vorticity for fluid elements (Casimir constants) but extreme filamentation.
- Statistical description by a local pdf: $\rho(\sigma,\mathbf{r})$

  σ vorticity value, $\mathbf{r}$ position, local normalisation $\int\rho(\sigma,\mathbf{r})\, d\sigma=1$

- Maximisation of a mixing entropy: $S=-\int\rho \ln\rho\, d^2\mathbf{r}$ with the constraint of energy conservation
- Energy is purely kinetic but can be expressed in terms of long range interactions:

  Mean field approximation:

  $-\Delta\psi=<\sigma>$ (ψ smooth)

  $E=\int\psi<\sigma>dxdy$, with $<\sigma>=\int\rho(\sigma,\mathbf{r})\,\sigma\, d\sigma$

Statistical equilibrium for a jet (confined to a channel)

Juttner, Thess, Sommeria (Phys. Fluids 1995)

- Straight (periodic) channel
- No beta effect
- No meridional topography: free x-wise translation

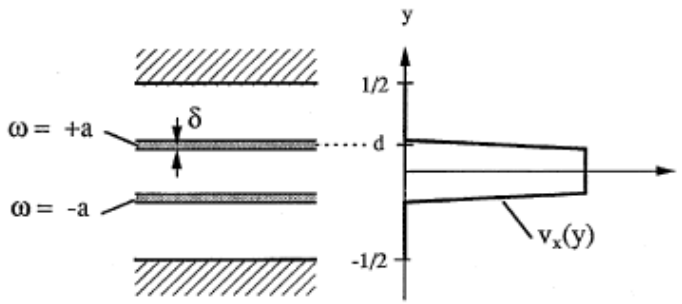

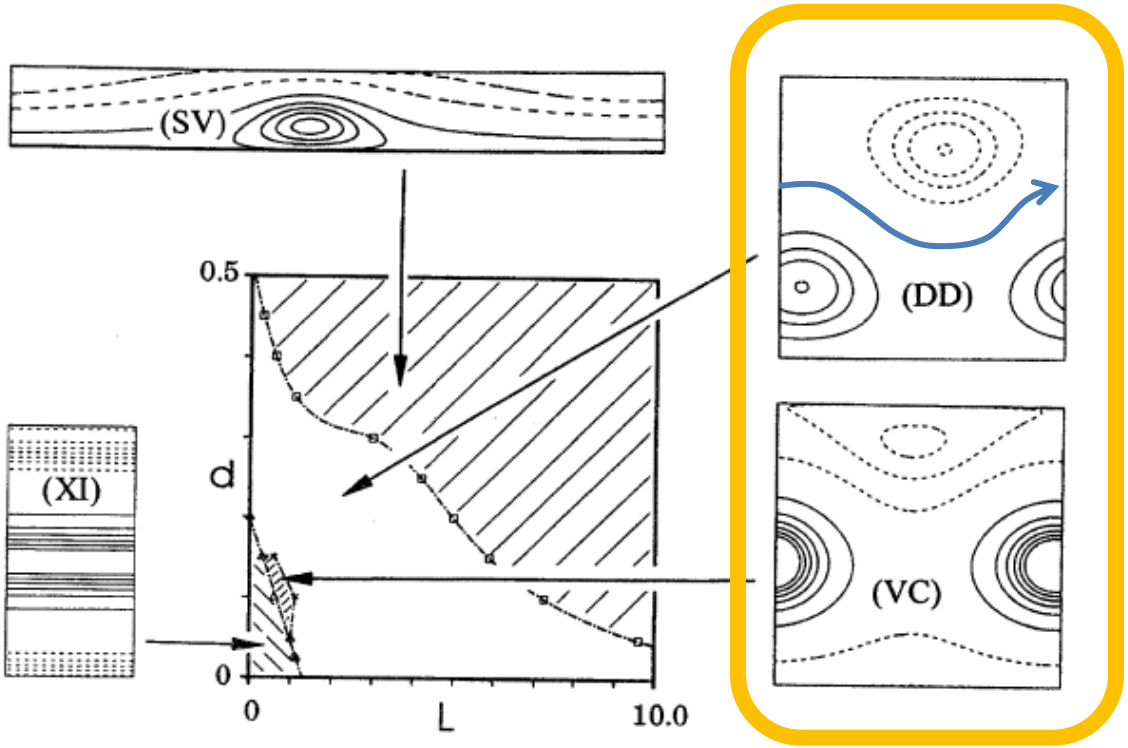

Saturn's hexagon

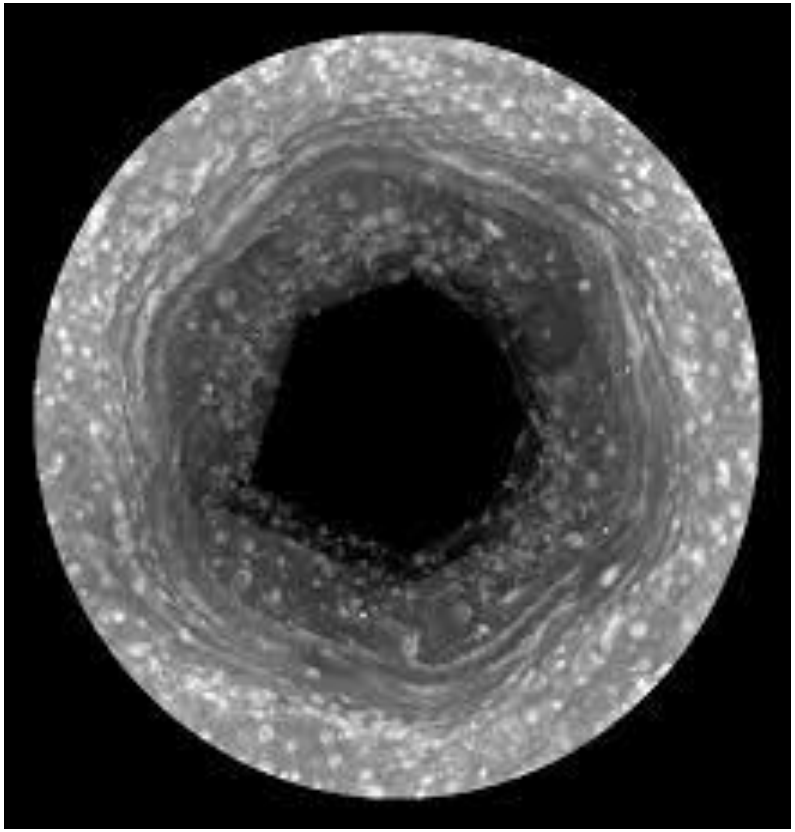

Jupiter's Great Red Spot

Bistability and reversals in the doubly periodic domain *F. Bouchet et E. Simmonet, 2009*

- Equilibrium statistical mechanics predicts a 2nd order phase transition between unidirectional and dipole flows

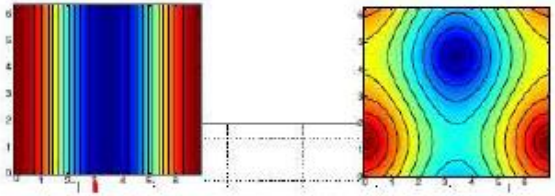

δ=1.02 **aspect ratio δ** δ=1.04

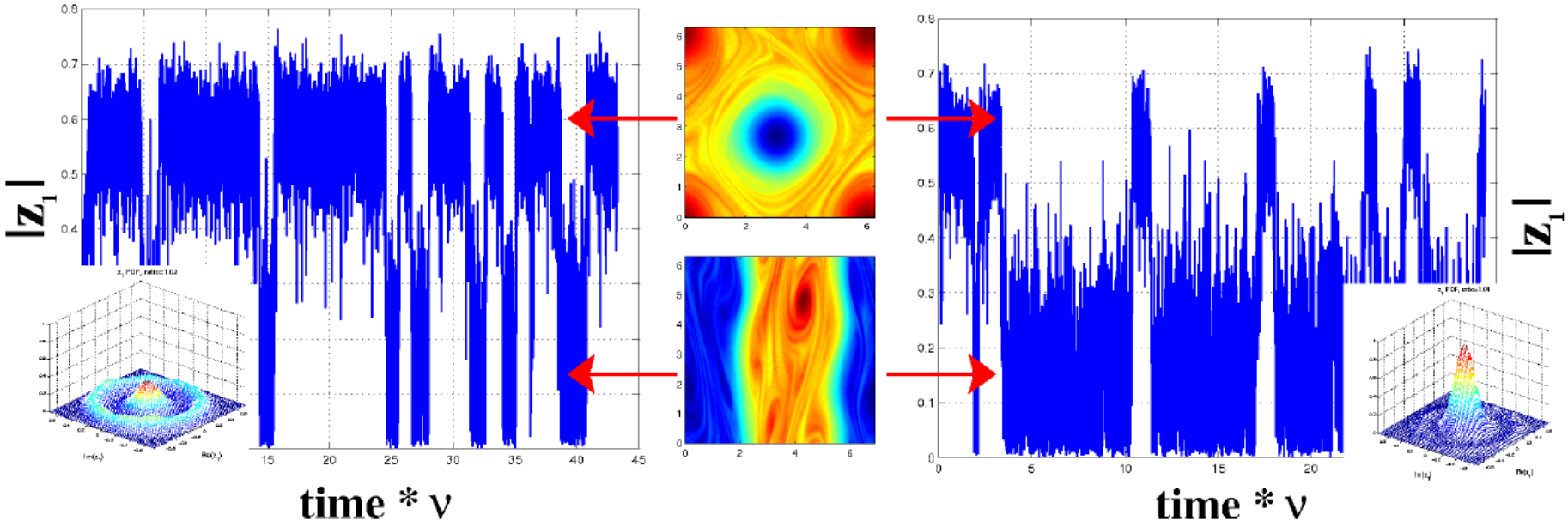

Bistability in a laboratory jet

Transitions Between Blocked and Zonal Flows in a Rotating Annulus with Topography

Eric R. Weeks, *et al.*

Science **278**, 1598 (1997);
DOI: 10.1126/science.278.5343.1598

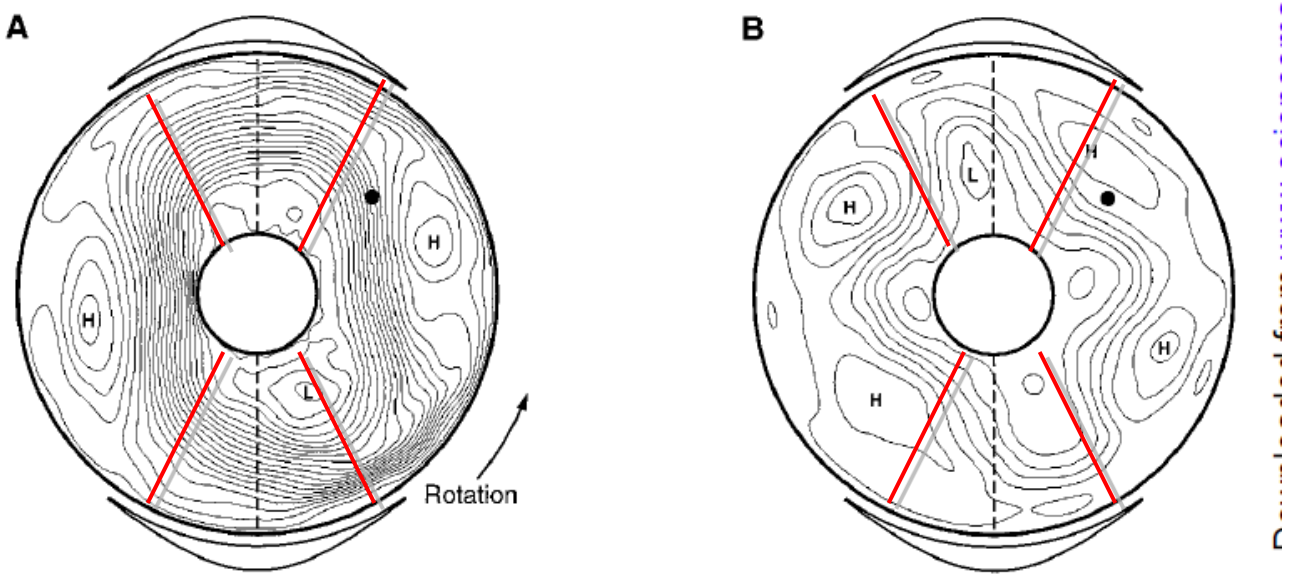

Fig. 2. Time-averaged stream function contours calculated from experimental data for (**A**) zonal and (**B**) blocked flow. The peaks of the ridges are indicated by dashed lines, and the profile of each ridge is shown by black curves outside the rim of the round panels. The contour interval is 15 $cm^2\ s^{-1}$ for both plots. The annulus rotates counterclockwise, and the flow is in the direction of rotation (eastward). The Rossby numbers *Ro* for the zonal and blocked flows are 0.33 ± 0.02 and 0.22 ± 0.02, respectively (pump flux $F = 390$ and 260 $cm^3\ s^{-1}$, respectively); for both flows, the Ekman number $Ek = 4.8 \times 10^{-4}$ ($\Omega = 3\pi$ rad s^{-1}). A video camera was used to track neutrally buoyant particles of 1 mm diameter, and time-averaged stream functions were determined by averaging the particle trajectories in time (*23*) and fitting the results to basis functions. The highs and lows of the stream function are indicated by bold letters H and L, respectively. The black dots indicate the horizontal location of the hot-film probe.

Transition between blocked and propagating states

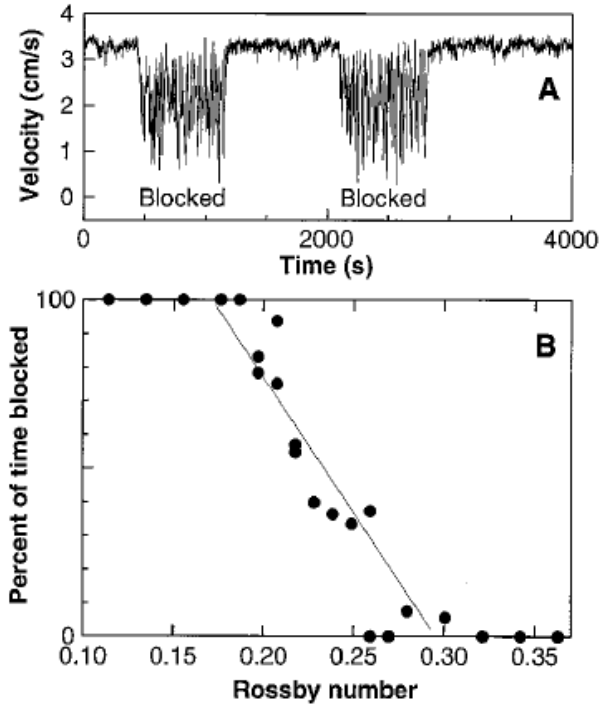

Fig. 5. (**A**) Velocity time series showing intermittent transitions between zonal and blocked flow (compare Figs. 3 and 4); $Ro = 0.237 \pm 0.005$ and $Ek = 4.8 \times 10^{-4}$ (pump flux $F = 280$ cm^3 s^{-1} and $\Omega = 3\pi$ rad s^{-1}). (**B**) The fraction of time spent in the blocked state as a function of the Rossby number [compare with similar plots for the atmosphere (*4*) and barotropic models (*12*)]; $Ek = 7.2 \times 10^{-4}$ ($\Omega = 2\pi$ rad s^{-1}). To guide the eye, the straight line shows the least-squares fit to the intermittent data.

Experimental set-up at LEGI

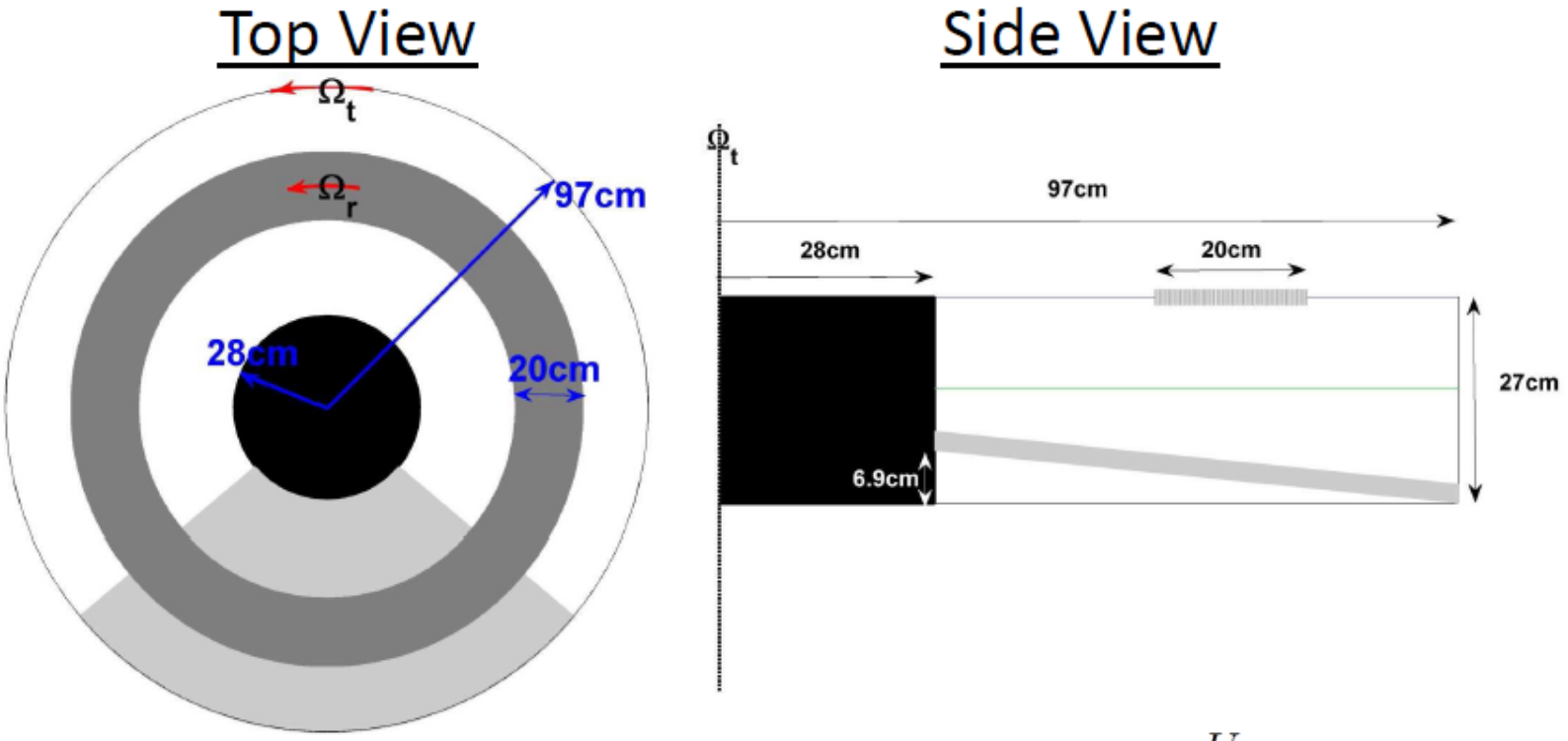

Typical Values: $\Omega_t \approx 0.4 - 0.6\ rad/s$

$\Omega_r \approx 0.78\ rad/s$

$\beta = \dfrac{2\Omega_t s}{H} \approx 0.37\ rad/s/m$

$Ro = \dfrac{U}{2\Omega_t L} \approx 2.6$

$Ek = (4\pi/H)^2(\nu/\Omega_t) \approx 0.0043$

$L_R = \dfrac{(gH)^{1/2}}{2\Omega_t} \approx 1.63m$

No meridional topography

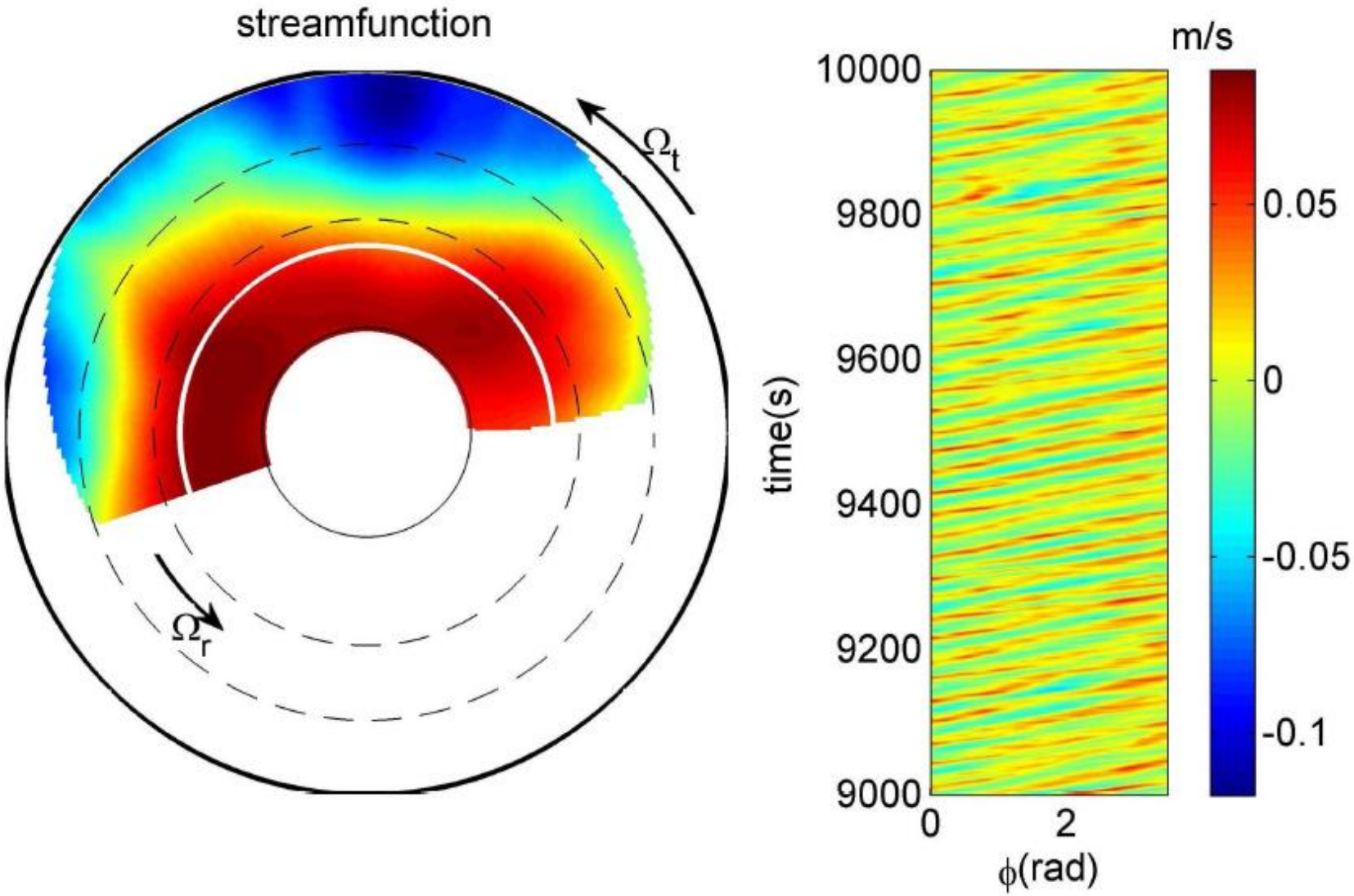

Meridional topography-> bistability

Same parameters

propagating

Ω_t increase

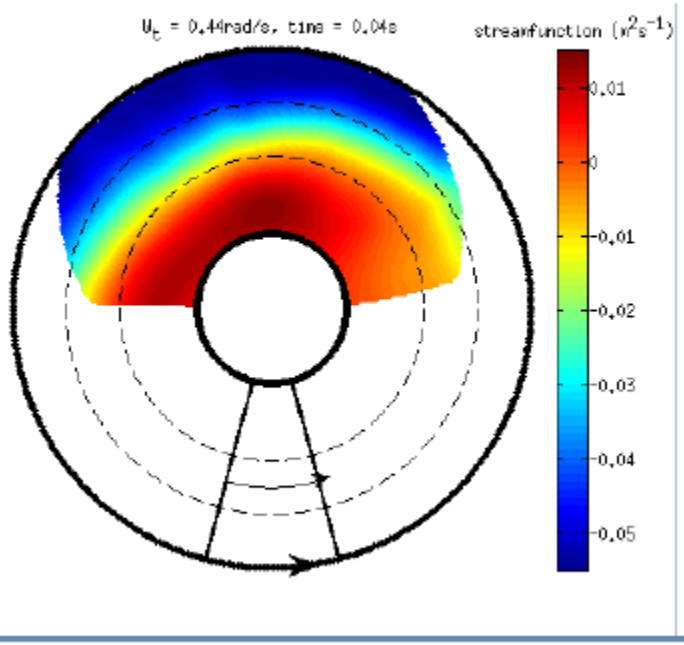

blocked

Ω_t decrease

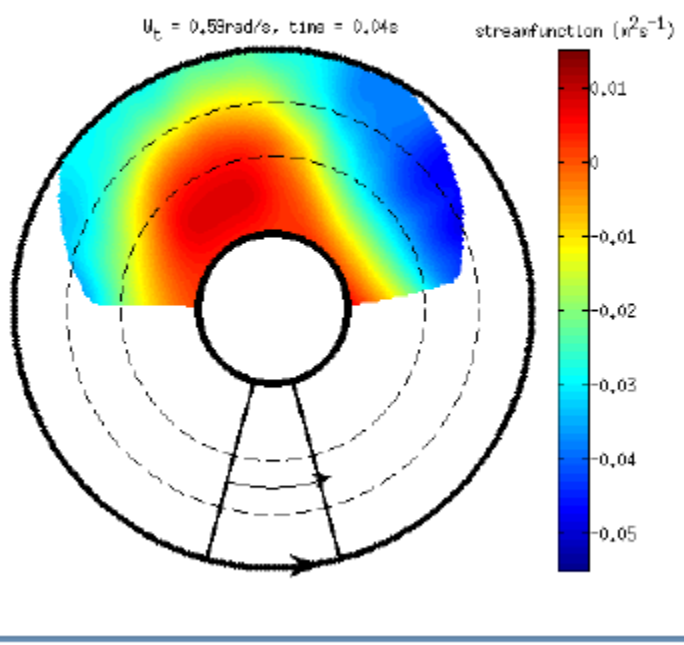

propagating

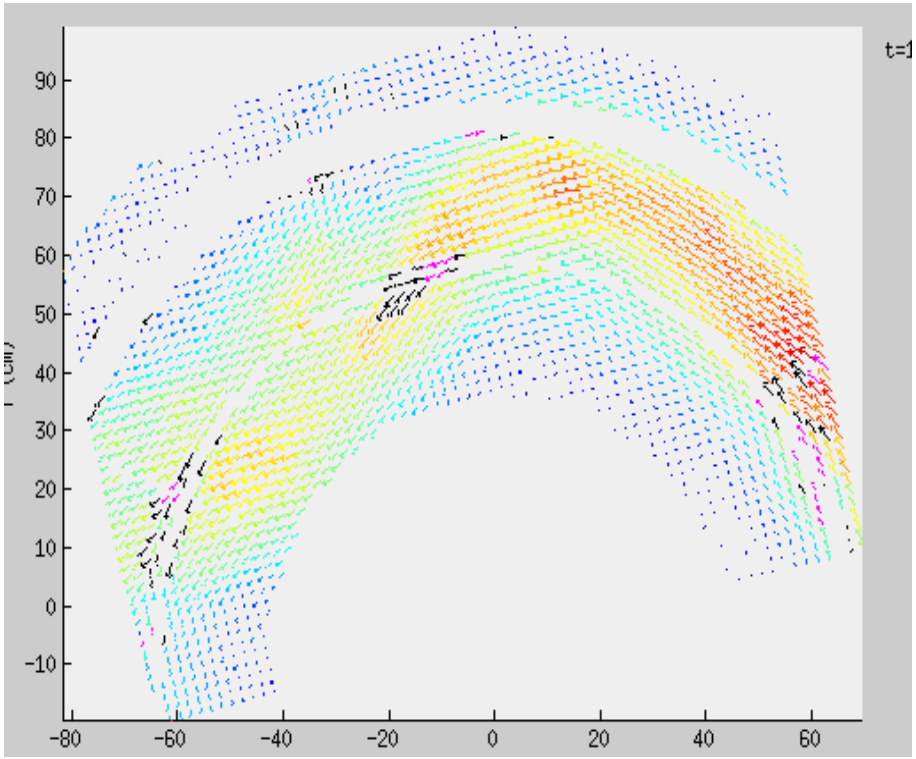

blocked

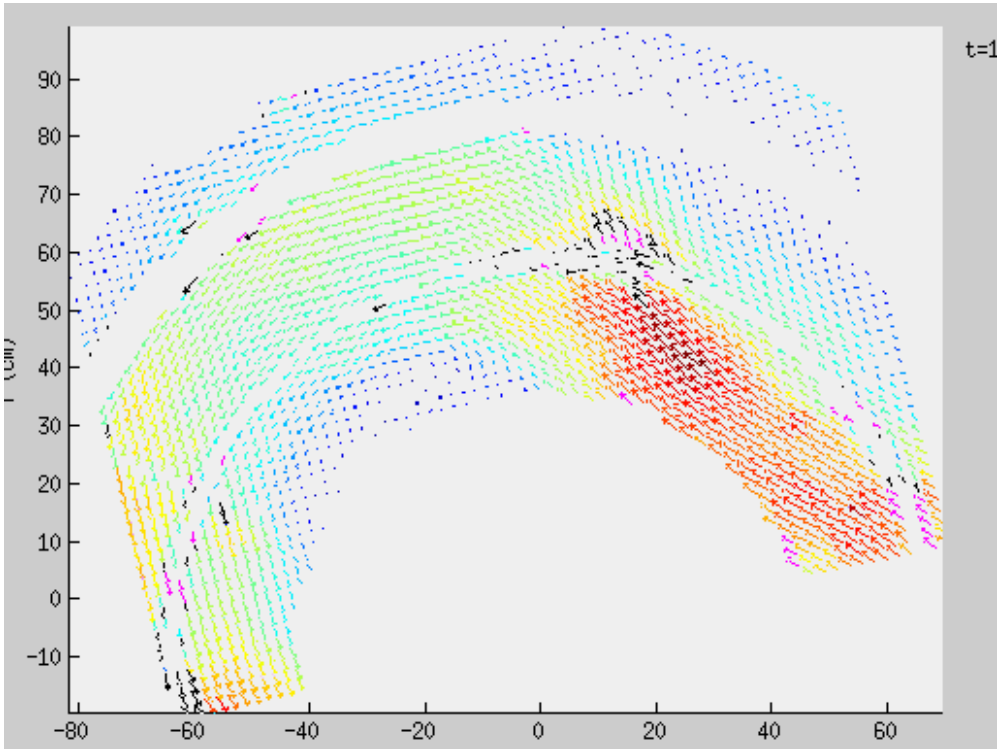

Analysis of Azimuthal Fourier modes

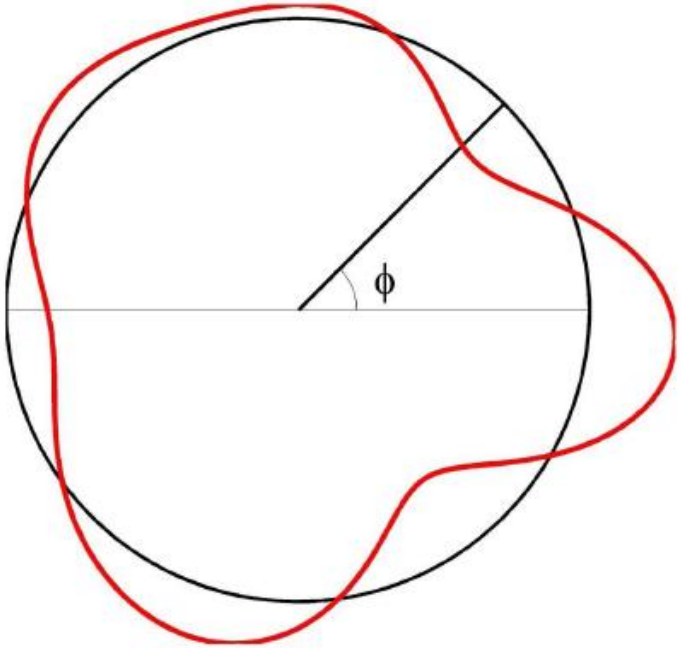

$$f(\phi) = A_1 e^{i\phi_1} e^{i\phi} + A_2 e^{i\phi_2} e^{2i\phi} + A_3 e^{i\phi_3} e^{3i\phi} + ...$$

$$f(\phi, t) = A_1(t) e^{i\phi_1(t)} e^{i\phi} + A_2(t) e^{i\phi_2(t)} e^{2i\phi} + A_3(t) e^{i\phi_3(t)} e^{3i\phi} + ...$$

purely propagating mode-3 wave: $< A_3(t) e^{i\phi_3(t)} > \; = \; 0$

standing mode-3 wave: $< A_3(t) e^{i\phi_3(t)} > \; = \; c_0$

Hysteresis: azimuthal mode n=3

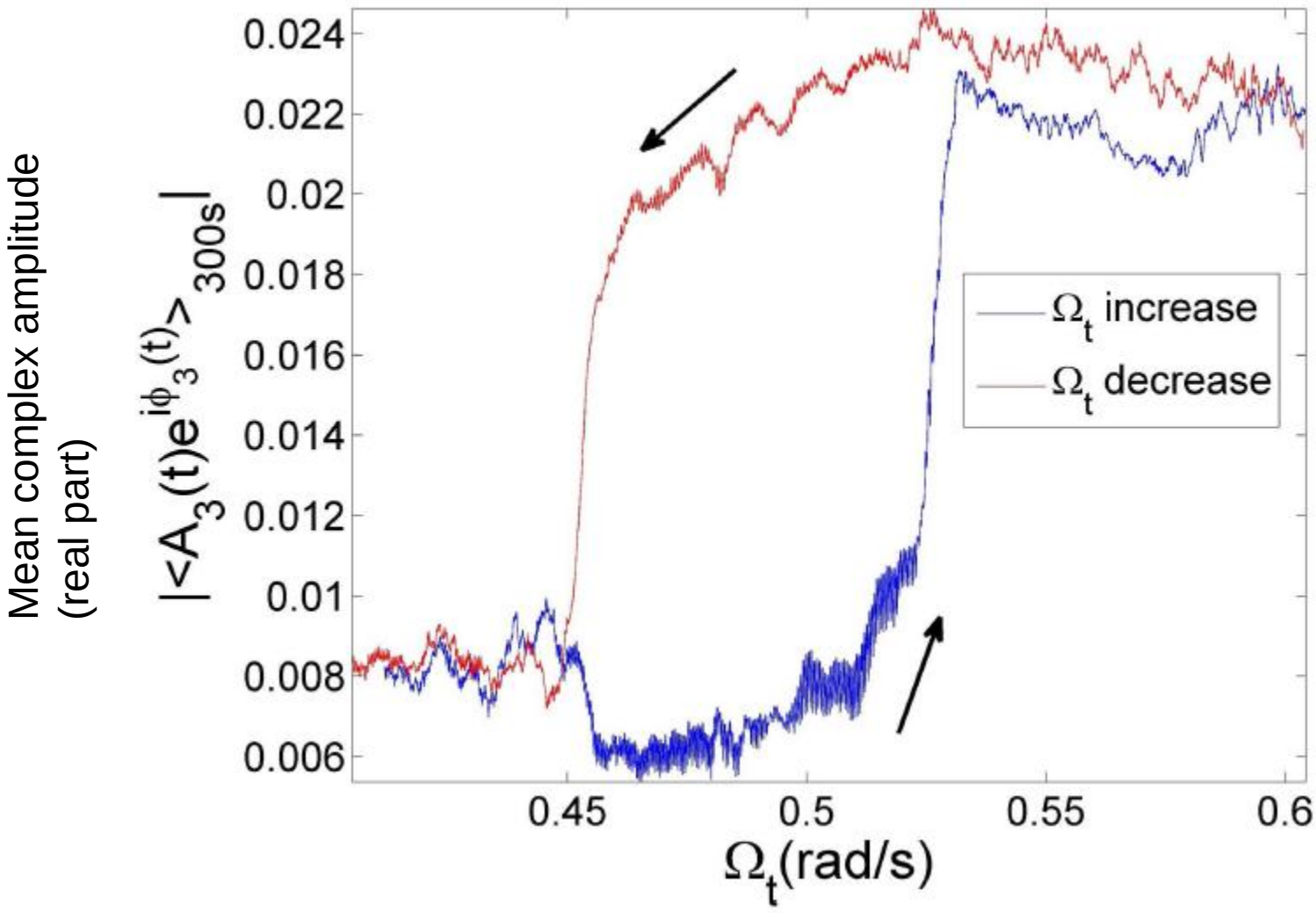

blocked

propagating

Third regime: random phase pinning

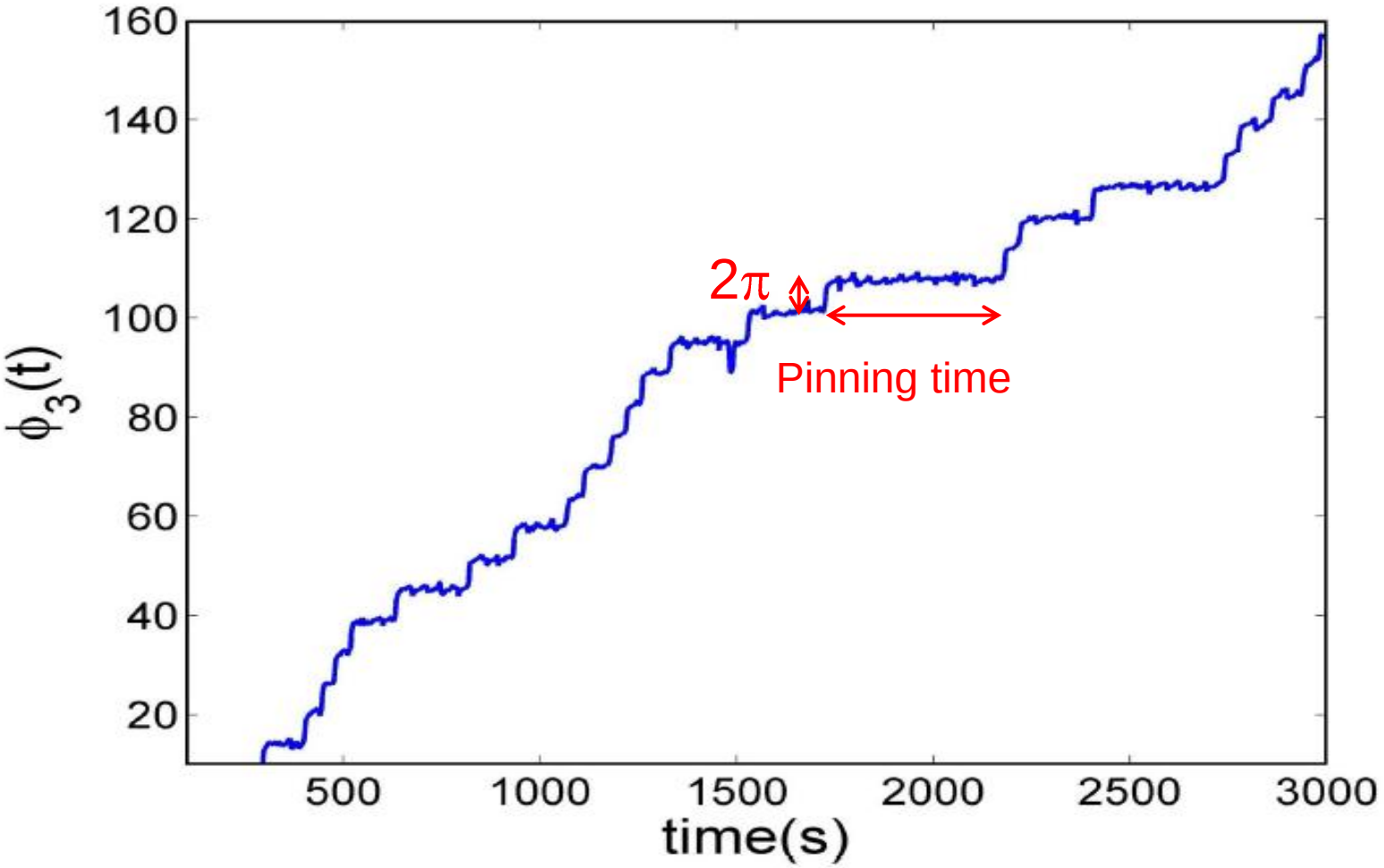

Random pinning time : no memory of previous step (cf. conditional probability)

Conclusions

- Bistability confirmed for azimuthal jets interacting with a meridional topography
- No switches observed in the new experiments: sensitivity to details in turbulence forcing ?
- A new regime with random phase pinning observed.

Theoretical challenges

- perturbation of a statistical equilibrium by a weak meridional topography ?
- Dynamics in the limit of weak forcing and dissipation ?
- Numerical modelling: predictability, sensitivity to lateral boundary layers …